The Role of Grain Boundaries in High Temperature Creep Fracture of an Oxide Dispersion Strengthened Superalloy

Harald Zeizinger* and Eduard Arzt

(Max-Planck-Institut für Metallforschung, Institut für Werkstoffwissenschaften, Seestraße 92, D-7000 Stuttgart 1)

Creep fracture of the oxide dispersion strengthened superalloy INCONEL MA 6000 has been investigated as a function of grain elongation and loading direction. Metallographic analysis reveals a high susceptibility to creep cavitation at grain boundaries perpendicular to the applied stress. The strong dependence of the rupture time on grain aspect ratio and stress direction is interpreted in terms of a model in which it is assumed that the extent of creep constraint on damage formation governs the fracture behaviour. It is concluded that for realizing the full potential of dispersion strengthening, fine grain regions must be eliminated.

Die Rolle von Korngrenzen beim Hochtemperaturkriechbruch einer oxiddispersionsgehärteten Superlegierung

Der Kriechbruch der oxiddispersionsgehärteten Superlegierung INCONEL MA 6000 wurde als Funktion der Kornstreckung und der Belastungsrichtung untersucht. Metallographische Beobachtungen zeigen eine starke Neigung zur Ausbildung von Kriechporen an Korngrenzen, die senkrecht zur äußeren Spannung liegen. Die starke Abhängigkeit der Bruchzeit von dem Kornstreckungsverhältnis und der Spannungsrichtung wird im Rahmen eines Modells interpretiert, das das Ausmaß der Behinderung der Schädigungsentwicklung durch benachbarte Körner als entscheidend für das Bruchverhalten annimmt. Es folgt, daß Feinkornbereiche vermieden werden müssen, um das volle Potential der Dispersionshärtung ausschöpfen zu können.

1 Introduction

Oxide dispersion strengthened (ODS) superalloys represent a modern class of high temperature alloys which are promising candidates for applications in both stationary gas turbines and aircraft engines. By adding dispersoid particles to a superalloy matrix, at least three strengthening mechanisms can be exploited: solid solution, precipitation and dispersion hardening. This superposition results in high strength over a wide temperature range, with dispersion hardening as the predominant mechanism at temperatures above about 900 °C[1][2]. The detailed mechanisms of dispersion strengthening at high temperatures have been investigated only recently, e.g.[3][4][5].

In such highly strengthened materials particular attention must be paid to potentially weakening microstructural elements. At high temperature it is often the grain boundaries, especially those with a perpendicular stress component, which are potential sources of damage. They act as efficient sources for vacancies which accumulate in grain boundary voids causing early intergranular fracture. In order to take full advantage of dispersion strengthening at high temperatures, this detrimental effect of grain boundaries must therefore be minimized. This is attempted by recrystallizing the superalloy to a coarse, elongated grain structure[2][6][7]. The grain boundaries become uncritical when a certain grain aspect ratio (ratio of length over width of an average grain) is consistently achieved during recrystallization[6][8]. This processing step is, however, not always totally successful: recrystallization defects in the form of fine grained regions embedded in an otherwise coarse grained structure occur frequently. In addition, under transverse loading many grain boundaries are under tension and intergranular fracture, accompanied by a dramatic decrease in lifetime, is expected to occur. The magnitude and mechanisms of these deleterious grain boundary effects, which will be important in high-temperature service, have not been studied extensively in ODS alloys.

This paper is designed to contribute to the understanding of grain boundary damage processes in the elongated grain structures which are typical of current ODS superalloys. Careful metallographic investigation of the distribution of the damage after creep in MA 6000 has lead to a model which predicts time-to-fracture as a function of the grain aspect ratio. In this way, the experimentally measured effects of grain elongation and of loading direction on the high temperature strength of highly strengthened grains will be interpreted in terms of damage mechanics.

2 Experimental

The material on which this study was performed is INCONEL MA 6000, with the chemical composition shown in Table 1. It contains about 50 vol.% of coherent γ' precipitates and 2.5 vol.% Y_2O_3 dispersoids. The commercially applied zone annealing treatment leads to grains of typical length 10 mm and a grain aspect ratio of 15. Results of an extensive microstructural study can be found in [10].

Table 1. Nominal chemical composition of MA 6000 (in wt.%).

Ni	Cr	Al	Ti	W	Mo	Ta	C	B	Zr	Y_2O_3
69	15	4.5	2.5	4	2	2	0.05	0.01	0.15	1.1

Samples from tensile creep tests under varying test conditions were analyzed by both SEM and optical microscopy. The creep tests had been partly interrupted tests and tests conducted until failure. Specimens of two creep series were available for metallographic investigations (see Fig. 1):

– longitudinal tests, at 850 °C in a stress range from 305 MPa to 330 MPa and at 950 °C in a stress range from 190

MPa to 215 MPa, on material with an average grain aspect ratio R of about 13,

– tests, at 950 °C and 230 MPa, on material with varying grain aspect ratio R (5 to 63) in extrusion direction (longitudinal) and tests normal to the extrusion direction (long transverse) at the same temperature and stress.

For macroscopic metallographic investigations the best results were obtained after mechanical grinding and polishing the sections, followed by etching with 10 ml H_2O, 10 ml Ethanol, 10 ml HCl and 2 g Cu_2SO_4. To reveal γ'-precipitates, a different etchant (93 ml H_2O, 5 ml HNO_3 and 2 ml HF) was used. Further details are to be found in [11]).

3 Results

3.1 Structural Inhomogeneities in Undeformed Material

Figure 2 shows a fine grain region which has incompletely recrystallized. EDX-Analysis in the SEM confirmed that the chemical composition of these recrystallization defects is identical with that of the matrix. Therefore these defects are indeed small grains and not chemical inhomogeneities. The only difference to the long grains is geometric: a lower grain aspect ratio, and in many instances, a different crystallographic orientation.

This sort of material defect, which must be considered typical of present alloy processing, occupies only a small volume fraction and may appear to be uncritical for creep. However, in these zones the grain aspect ratio is locally decreased and – as will be shown below – cavitation on such grain boundaries may be enhanced. If the distribution of these defects is inhomogeneous, it is likely that some of the damaged grain boundaries will be close enough to allow coalescence to longer cracks. Metallographic analy-
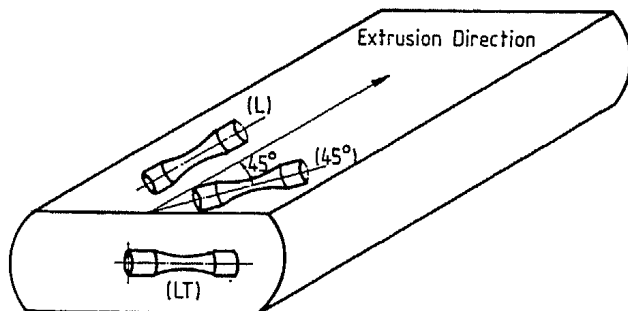

Fig. 1. Orientation of longitudinal (L), long transverse (LT) and 45° specimens (45°) with respect to the direction of grain elongation (extrusion direction).

Fig. 2. Typical recrystallization defect in the alloy investigated.

sis shows that microcracks on grain boundaries and also transgranular cracks are normally linked with such recrystallization defects in samples with an otherwise high grain aspect ratio.

3.2 Metallographic Damage Analysis

Figures 3 and 4 are SEM micrographs of the fracture surfaces after different creep tests. The first two pictures (Fig. 3) show the fracture surfaces of specimens crept in the longitudinal direction. Figure 3a represents a test at 950 °C and 230 MPa with material of a grain aspect ratio $R = 5$. Fracture is typically intergranular with the pull-out of single grains. The grain diameters correspond to those measured from cross-sections of the same specimen. In contrast, Fig. 3b is the fracture surface of the sample with a high grain aspect ratio ($R = 63$), tested under identical conditions as before. Fracture is transgranular here, with the fracture plane running at approximately 45° with respect to the stress direction.

Figure 4a shows the fracture surface of a long transverse test. In contrast to the longitudinal tests the long grain
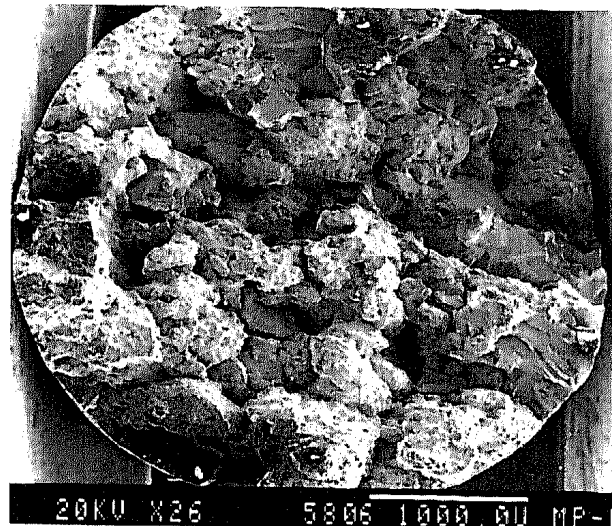

Fig. 3a. $R = 5$, time-to-fracture $t_f = 0.4$ h. Fracture is intergranular with typical pull-out of single grains.
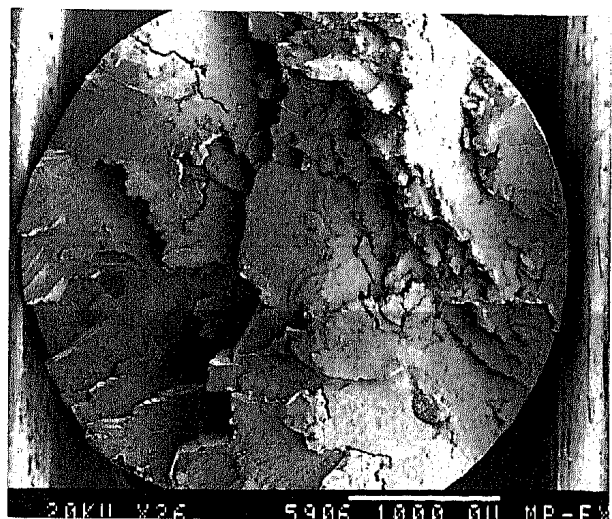

Fig. 3b. $R = 63$, $t_f = 171$ h. Fracture is completely transgranular. The crack plane runs at approximately 45° with respect to the stress direction.

Fig. 3a and b.   Fracture surfaces of creep specimens in longitudinal direction with different grain aspect ratio R ($T = 950$ °C, $\sigma = 230$ MPa).

boundaries now act as transverse grain boundaries leading to the typical intergranular fracture. In Fig. 4b the stress direction was 45° with respect to the extrusion direction. Figures 4a and b clearly reveal the fibre-like grain structure on the fracture surface. The smooth areas in the fracture surfaces are the result of the final fast fracture which occurs transgranularly.

Figure 5a shows the fraction of intergranular fracture surface as a function of the grain aspect ratio. Thus, the fracture mode changes to transgranular above a grain aspect ratio of about 18. Although only 4 samples with varying grain aspect ratio were available for analyzing the fracture mode, the transition from inter- to transgranular fracture seems well documented.

The change in fracture mode with increasing grain aspect ratio is accompanied by a dramatically increasing time-to-fracture (Fig. 5b). An increase of the grain aspect ratio from
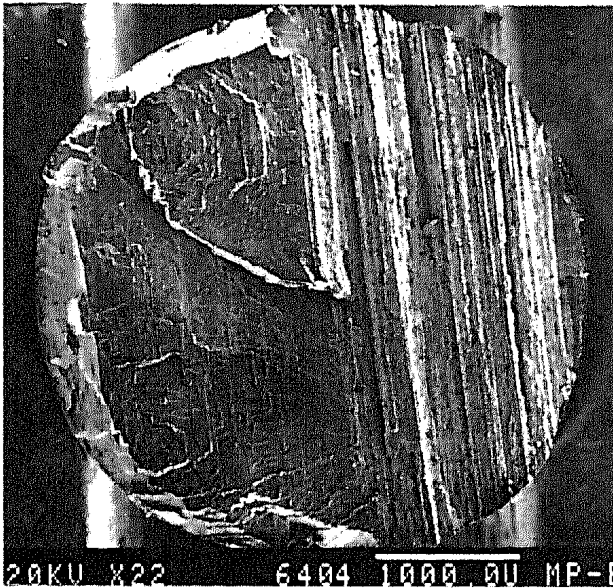

Fig. 5a.   Intergranular fraction of the fracture surface area.

Fig. 4a.   Long transverse test: "effective" $R \approx 1$, $T = 950$ °C, $\sigma = 230$ MPa and $t_f = 0.16$ h.

Fig. 5b.   Rupture time. The open square at $R = 3$ represents a long transverse test with an "effective" $R \approx 3$ (longitudinal data from Arzt and Singer[8]), transverse data from Zeizinger and Wilkinson[12]).

Fig. 5a and b.   Fracture properties as a function of the grain aspect ratio R; $T = 950$ °C, $\sigma = 230$ MPa.
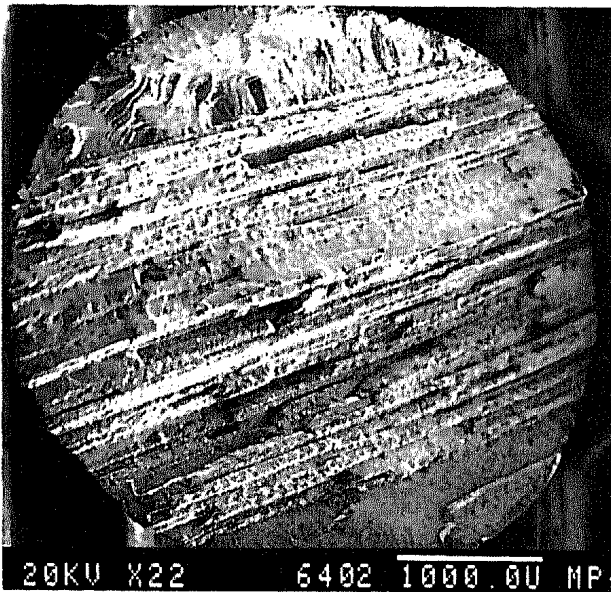

Fig. 4b.   45° test: "effective" $R \approx 1$, $T = 950$ °C, $\sigma = 230$ MPa and $t_f = 23.55$ h.

Fig. 4a and b.   Fracture surfaces of long transverse and 45° specimens. The grain aspect ratio in extrusion direction was about 13. Both micrographs clearly reveal the fibre-like grain structure.
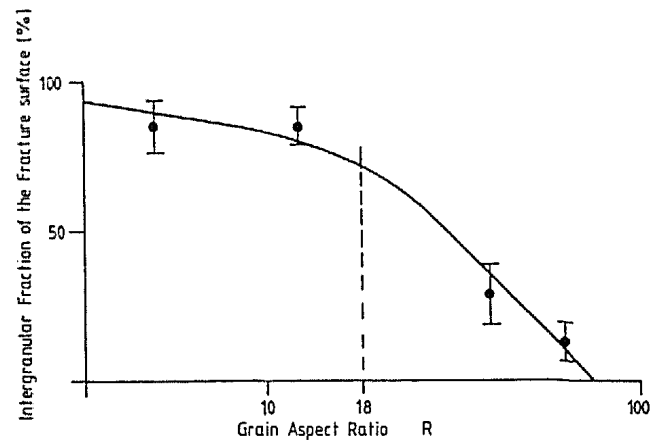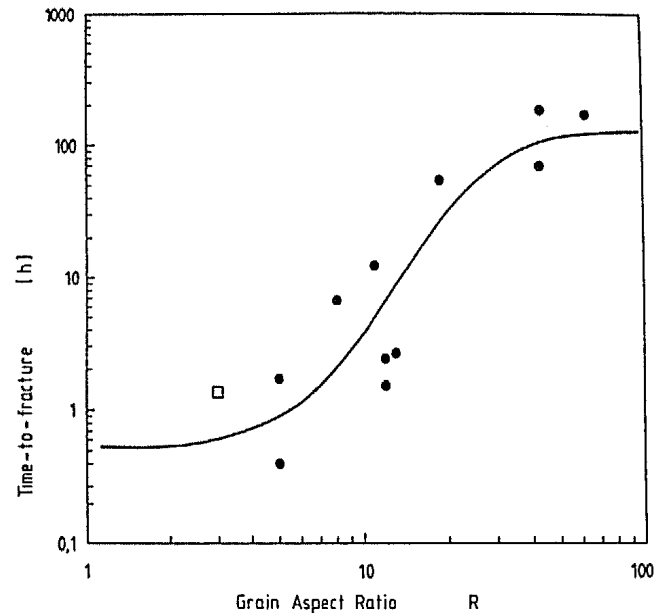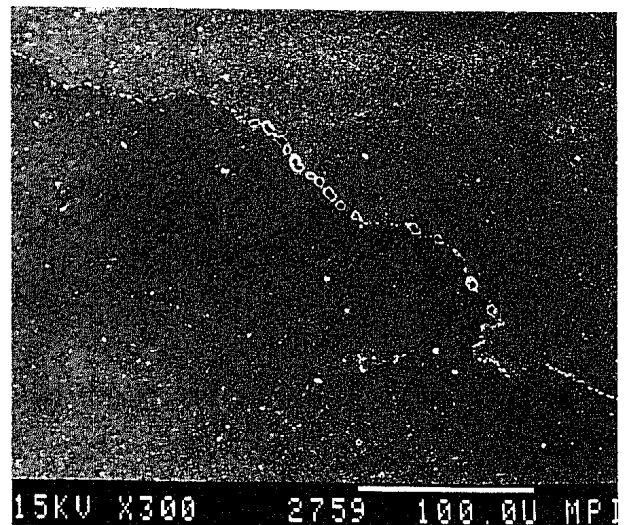

Fig. 6.   Voids on grain boundaries with a normal stress component. Grain boundaries parallel to the stress direction are undamaged (horizontal stress orientation in this figure). Longitudinal test: $R = 5$, $T = 950$ °C, $\sigma = 230$ MPa and $t_f = 0.4$ h.

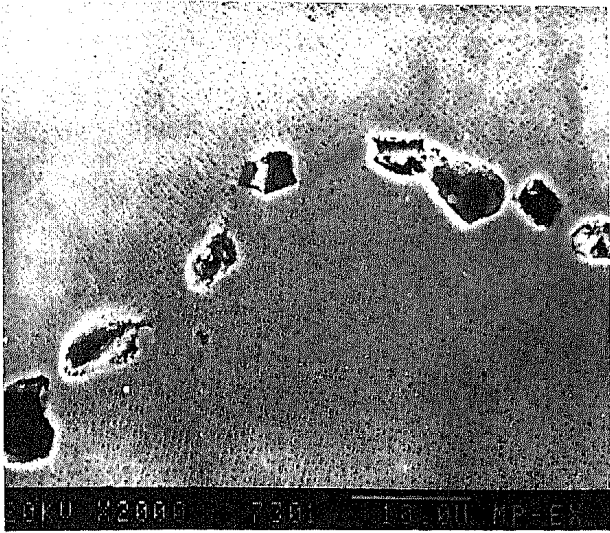Fig. 7. γ'-free diffusion zone between grain boundary voids pointing to grain boundary diffusion as the dominant growth mechanism (stress direction vertical).
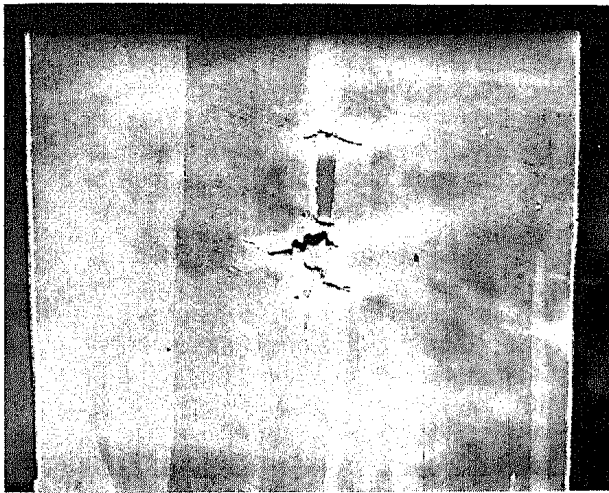

Fig. 8.   Section of a specimen crept in the longitudinal direction. In regions with locally decreased grain aspect ratio grain boundaries are damaged by microcracks.
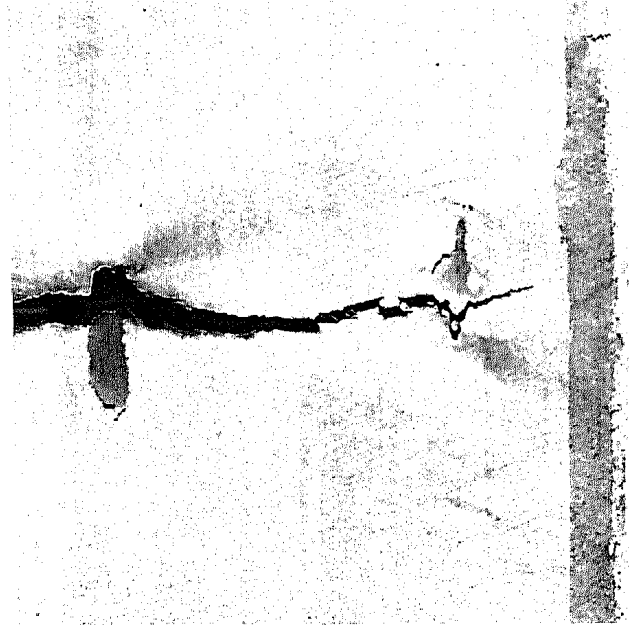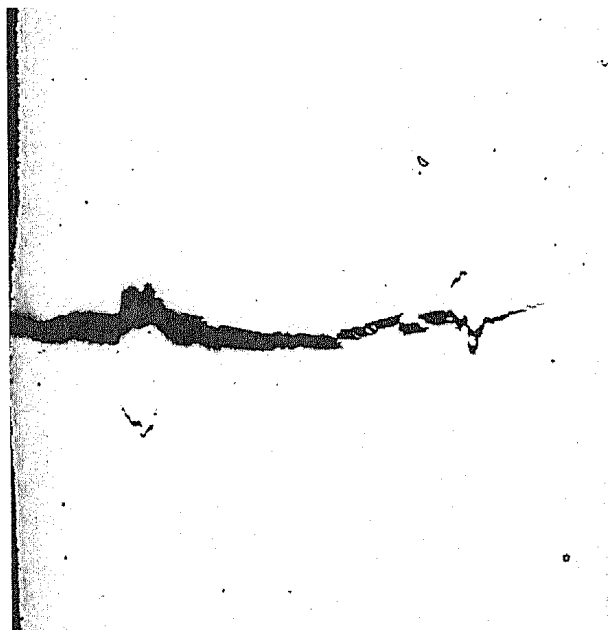
1 to 20 causes a prolongation of the rupture life by a factor of 100. For grain aspect ratios higher than 20 no significant increase in fracture time can be observed. The square at $R \approx 3$ (Fig. 5b) represents a long transverse test[12]; in such a plot this data point fits well within the scatterband of the longitudinal data.

The mechanism for intergranular failure of MA 6000 is damage by void growth on grain boundaries with a normal stress component. Figure 6 shows typical grain boundary voids, which disappear wherever the boundary's tangent becomes parallel to the applied stress (horizontal in the figure). On grain boundaries parallel to the stress axis no voids could be found. The spherical shape of the voids points to grain boundary diffusion as the dominant growth mechanism. The specimen in Fig. 7 was etched for γ'-precipitates, which show as small rectangular holes in the matrix. Between the voids on the grain boundary a γ'-free zone appears, which is an additional indication for void growth by diffusion.

Another observation is related to the distribution of cavitated grain boundaries. At low grain aspect ratio (also for the transverse test direction with the low "effective" grain aspect ratio) the transverse grain boundaries which have cavitated were found to be homogeneously distributed. With increasing grain aspect ratio the distribution of cavitated facets becomes more inhomogeneous. At high grain aspect ratio voids or microcracks occur only in regions with a low "local" grain aspect (Fig. 8).

3.3   Damage Accommodation: Grain-Boundary Sliding vs. Power-Law Creep

The growth of grain boundary voids requires accommodation of the material in the vicinity of the damaged grain boundary. Different accommodation mechanisms are possible: accommodation by grain boundary sliding[8][13]) or by plastic deformation of the adjacent grains[13][14]). Obviously in both cases the grain aspect ratio plays an important role for the accommodation process. With increasing grain aspect ratio the shear stress on longitudinal boundaries due to cavity growth on transverse boundaries will decrease and accommodation by grain boundary sliding

Fig. 9a and b.   Linkage of grain boundary microcracks at grains with low grain aspect ratio by a transgranular crack; (a) unetched and (b) etched.
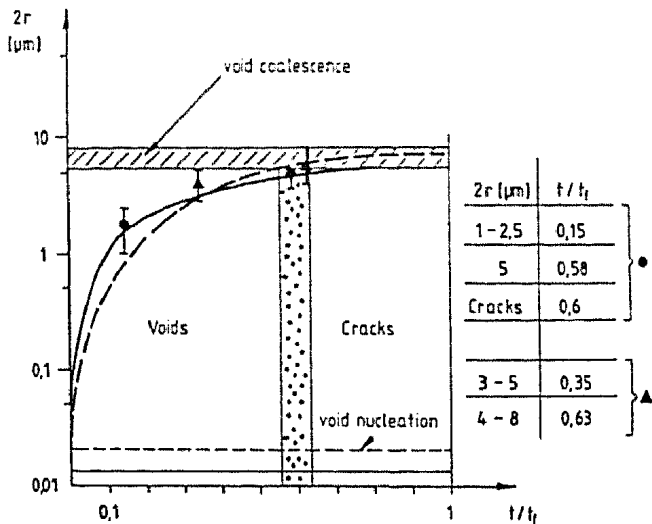
Fig. 10. Average void diameter as a function of time normalized to the rupture time. Interrupted tests: $R \approx 13$, 190 MPa and 950 °C (triangles), 305 MPa and 850 °C (circles).
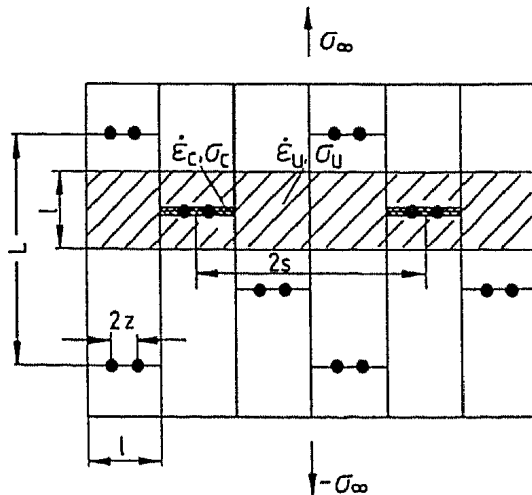

Fig. 11. Schematic grain configuration with constant grain aspect ratio $R = L/l$. The properties with subscript c relate to the damaged, those with subscript u to the undamaged regions. σ_∞ is the applied tensile stress.
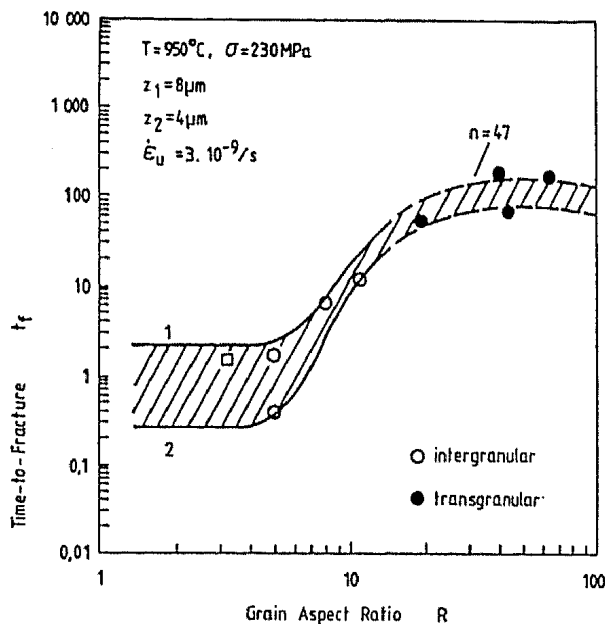

Fig. 12. Comparison of the calculated rupture time as a function of grain aspect ratio (Eq. (1)) with the experimental data (see text for more details).

becomes more difficult[15]). At the same time more creep deformation will be necessary for accommodation because there are fewer damaged grain boundaries (see model below). In both cases the constraint on void growth increases with increasing grain aspect ratio.

To decide experimentally which of the two accommodation mechanisms is more likely in MA 6000, creep tests were carried out in compression, with samples marked by surface scratches. The stress direction was 45° to the extrusion direction. Thus the long grain boundaries were loaded under maximum shear stress and measurable grain boundary sliding could be expected. Yet at all test conditions (same temperature and stress range as for the tensile creep tests) no displacement of the surface scratches could be observed. We therefore conclude that under these test conditions the accommodation is unlikely to occur by grain boundary sliding.

3.4 Fracture Process

Final fracture takes place by the linking-up of the intergranularly damaged regions. Figure 9 shows how transgranular fracture at high grain aspect ratio is initiated at recrystallization defects with a low "local" grain aspect ratio where separate intergranular microcracks have developed by cavitation. The samples investigated showed only a few of the resulting macrocracks. The reasons are: first, the low density of recrystallization defects and second, the primary macrocrack grows at the expense of all other forming cracks.

To gain information on the fraction of creep life spent in forming intergranular cracks, the void diameters were measured on sections of samples subjected to interrupted tests under selected conditions. The average void diameter $2r$ as a function of the creep time t normalized to the rupture time t_f is shown in Fig. 10. For times less than about 60 % of the rupture time, separate voids are found while for longer times all voids are coalesced to microcracks on transverse grain boundaries. The cavity nucleation time (the time for voids to exceed the "sinter-radius" $r = 2\gamma/\sigma$, where γ is the surface energy per unit area and σ is the tensile stress) can be estimated at less than 10 % of the rupture time.

4 Model for Time-to-Fracture as a Function of Grain Aspect Ratio

On the basis of the metallographic observations, a model for the evolution of intergranular damage in elongated grain structures was developed. It rests on the following main assumptions (see also Fig. 11):

– cavities nucleate and grow on grain boundaries with a normal stress component,

– void growth occurs by grain boundary diffusion,

– grain boundary sliding along grain boundaries parallel to the stress direction is suppressed,

– void growth is accommodated by power law creep in the surrounding grains,

– the time-to-fracture can be approximated by the calculated time for cavity coalescence.

Adaptation of the model for constrained cavity growth by Cocks and Ashby[13] to the present grain geometry leads to the following expression for the theoretical time-to-fracture (see Appendix):

$$t_f = \frac{0.085 \, k \, T}{\delta_B \, D_B \, \Omega} \frac{z^3}{\sigma_\infty} \left[1 - (1 - \frac{1}{R})^n \right] + \frac{\varepsilon_B}{\dot{\varepsilon}_u} (1 - \frac{1}{R})^n \quad (R \gtrless 1) \quad (1)$$

where R is the grain aspect ratio, n the stress exponent for power law creep (Eq. A2), $2z$ the average spacing of cavities on a cavitated grain boundary, σ_∞ the remote applied stress, $\delta_B D_B$ the thickness times diffusivity of the grain boundary, Ω the atomic volume, ε_B the total strain due to void growth and $\dot{\varepsilon}_u$ the creep rate of uncavitated material (Eq. A2).

This equation consists of two terms weighted by factors which depend on the grain aspect ratio. The first term, which predominates at low grain aspect ratio, describes unconstrained void growth. With increasing grain aspect ratio the second term becomes important; Eq. (1) then converges to a Monkman-Grant type relation. An equation of similar form has been obtained by using a tensile-crack model for the grain boundary facet cavitating under constrained conditions (see e.g. Riedel[16]). It is important to note that the present model contains the grain aspect ratio as the decisive parameter which determines the extent of creep accommodation necessary for cavity growth.

In Fig. 12 the measured rupture time as a function of the grain aspect ratio (symbols) is compared with calculated fracture time (lines). The stress exponent $n = 47$ was taken from Howson et al.[17]. For the void spacing $2z$, the range between 8 and 16 μm was assumed, which corresponds to values measured on longitudinal sections of crept specimens.

Figure 12 shows that the model is in good agreement with experimental data over the whole range of grain aspect ratios. While the agreement in absolute values, especially at high grain aspect ratios, may in fact be fortuitous (see discussion below), the plot suggests that the general trend of rupture time improvement with increasing grain elongation can indeed be due to the increasing constraint on void growth. The agreement between theory and experiment will be further discussed below.

5 Discussion

Even in the relatively coarse-grained ODS materials investigated in this study, grain boundaries play an important role in high-temperature deformation and fracture. It has been shown that the grain boundaries become susceptible to damage formation whenever the grain elongation in the direction of loading is small, i.e. when the grain aspect ratio is insufficient or when a fully recrystallized material is subjected to stresses at an angle to the extrusion direction. In both cases, cavities form readily on grain boundaries with a perpendicular stress component, with typical nucleation times smaller than 10 % of the time-to-fracture.

This high susceptibility to intergranular damage formation must be attributed to the relative weakness of the grain boundaries in comparison with the highly strengthened grain interiors of MA 6000. The particle-free zones between the cavities suggest that the primary void growth mechanism is diffusion, which is not affected by the presence of dispersoids (apart from a possible effect on vacancy emission in the remaining grain boundary ligament – see e.g. Arzt et al.[18] – which is insignificant at the stresses considered). Also the testing temperatures – like the service temperatures foreseen for such alloys – are higher than for conventional high-temperature alloys, typically 80 % of the absolute solidus temperature; and

therefore diffusion rates, which depend mainly on the homologous temperature, are high.

The creep tests performed with the longitudinal grain boundaries oriented in the direction of maximum shear stress have shown that the accommodation of the local strain generated by void growth is unlikely to occur by grain boundary sliding, contrary to earlier suggestions[8]. The reason must lie in the highly serrated longitudinal grain boundaries, whose sliding displacement requires diffusion over long distances. Also, diffusion creep can be neglected as an accommodation process because the diffusion distance, which scales roughly with the length of the grains under longitudinal loading, is too large. Transverse loading, by contrast, does indeed give rise to considerable diffusion creep as has been shown recently[19].

These considerations leave power-law creep as the only realistic accommodation process. Based on earlier theories (e.g. Cocks and Ashby[13]), the model for the coupling between diffusional cavity growth and power-law creep in the undamaged grains has been adapted for the particular case of an elongated grain structure. It attributes the dramatic improvement in the fracture time with increasing grain aspect ratio to the increasing necessity of accommodating the strain accumulated by damage formation. In a grain structure with low aspect ratio, in which cavitation is relatively homogeneously distributed, accommodation plays a lesser role than in a high grain aspect ratio structure, where few cavitated grain boundaries are present. For void growth on the comparatively flat longitudinal boundaries under transverse loading, the accommodation is in fact negligible. This can explain why the rupture times in the transverse direction are so much inferior to those obtained in longitudinal tests.

The model agrees quite well with experimental results, especially at low grain aspect ratios. However, because the void spacing ($2z$), which can only be determined experimentally, enters Eq. (1) as a critical variable, the model is not fully predictive. Using sensible values for z, at least a correct order-of-magnitude estimate is obtained. Obviously, comparison between theory and experiment would be necessary at different stress levels. The model would predict a low stress sensivity at low grain aspect ratio as compared to longitudinal tests on high grain aspect ratio material. First creep results of transverse tests at different applied stresses[12][19] do indeed show a reduced stress dependence. However, the stress sensitivity m (where $t_f \sim \sigma^{-m}$) is typically different from the predicted $m = -1$. The reason may be that additional mechanisms, such as continuous void coalescence and/or nucleation give rise to a non-linear stress dependence even in the case of unconstrained cavity growth. This has been shown recently by Wilkinson[20], whose calculations lead to slopes between -1 and $-n$ (where n is the power-law creep exponent). A full model, which would have to incorporate this effect, has not yet been attempted.

The calculations show that the grain aspect ratio, rather than the grain size, determines the fracture path and thus the fracture time. This is reflected in the data of Fig. 5, although it must be realized that, due to the nature of the recrystallization process, grain aspect ratio and grain size could not be varied independently. The conclusion that at high temperature the grain shape effect "swamps any grain size effect" has already been drawn for thoriated nickel alloys by Wilcox and Clauer[9]. Their qualitative interpretation however relied on grain boundary sliding, which we have ruled out for the alloy considered here.

Strictly speaking, it is not the grain aspect ratio as such which is decisive for damage formation. Rather the interlocking between individual grains improves with increasing grain aspect ratio, which necessitates more damage accommodation in grains adjacent to a transverse grain boundary. An extremely disadvantageous case in which this interlocking is lost would be a planar boundary through the specimen as it can form e.g. when diffusion bonding is carried out in the coarse-grained state. Such a boundary, which would represent a low grain aspect ratio situation, would cavitate and fail rapidly, even if the aspect ratio of the neighbouring grains were high. Rupture times of such a joined part would therefore be expected to lie on the lower part of the curve in Fig. 12. A similar case of almost planar grain boundaries being subjected to tensile stresses arises in transverse testing. It is seen in Fig. 12 that the corresponding data point fits nicely into the rest of the data when the appropriate low grain aspect ratio in this direction is used. The low transverse rupture strength, and also the low creep ductility in this direction, can thus be attributed to the lack of creep constraint on damage formation.

While the initial transition to transgranular fracture seems to be well described by the model, the agreement at higher aspect ratios must be considered fortuitous. Formally, Eq. (1) reduces to a Monkman-Grant type relation in this limit. But the model, which explicitly describes cavitation and its accommodation, does not of course apply to predominantly transgranular failure. In particular, an inconsistency common to all cavitation models arises in this constrained case: the time-to-failure will not be determined only by cavity coalescence, but also by the joining of individual microcracks. This point has been emphasized by Riedel[21]. The statistical distribution of fine-grained regions, which act as nucleation sites for microcracks, would therefore have to be taken into account. Such a model has not yet been developed.

6 Conclusion

The results of the metallographic examination of crept specimens with different grain aspect ratios lead to the following picture of high temperature fracture in INCONEL MA 6000 (see also Fig. 13). Below a minimum grain aspect ratio ($R \leqq 10$) and under transverse loading, fracture is – apart from transgranular contributions to final fracture – completely intergranular. In this range creep cavities form and grow on grain boundaries with a perpendicular stress component. Beyond a small transition region ($10 \leqq R \leqq 15$) the fracture mode changes to predominantly transgranular. Our observations suggest that in this case fracture is initiated at the recrystallization defects, which are always present in the form of fine grain regions. These results can be explained by considering the necessity of accommodation processes for cavity formation: at lower grain aspect ratio and under transverse loading, creep accommodation plays a lesser role than at high grain elongation. A model for this process has been formulated on the basis of current cavitation theories, which, despite some remaining problems, correctly describes the trends observed.

From a practical point of view, the most important result is the high susceptibility of ODS alloys to intergranular damage formation. Fine grain regions are particularly vulnerable – even more so under conditions of high temperature fatigue[22][23]. Efforts to eliminate such recrystallization defects appear therefore to be indispensable.

7 Appendix

Calculation of the Time-to-Fracture as a Function of Grain Aspect Ratio R

Consider an idealized structure with grain aspect ratio $R = L/l$ (Fig. 11). The voids are homogeneously distributed on transverse grain boundaries (normal to the stress direction). The area fraction of voids is $f = r^2/z^2$ (with r = void radius and $2z$ = planar void spacing). Due to the diffusion of atoms from the void surface into the grain boundary corresponding grains are jacked apart. We assume that this separation in longitudinal direction (parallel to the stress direction) is accommodated by dislocation creep in adjacent grains. The structure of the derivation follows that by Cocks and Ashby[13].

Fig. 13a.   Void nucleation and growth on transverse grain boundaries in fine grain regions.
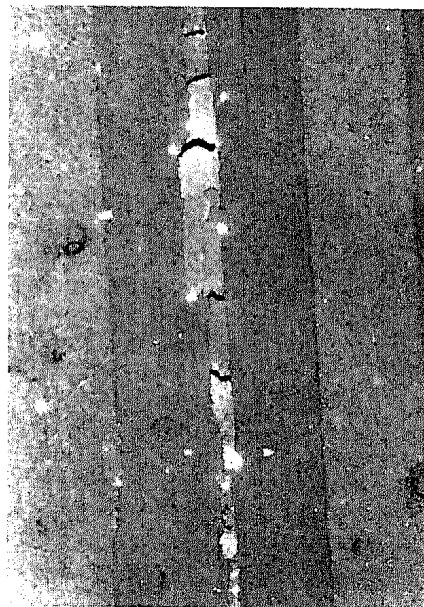
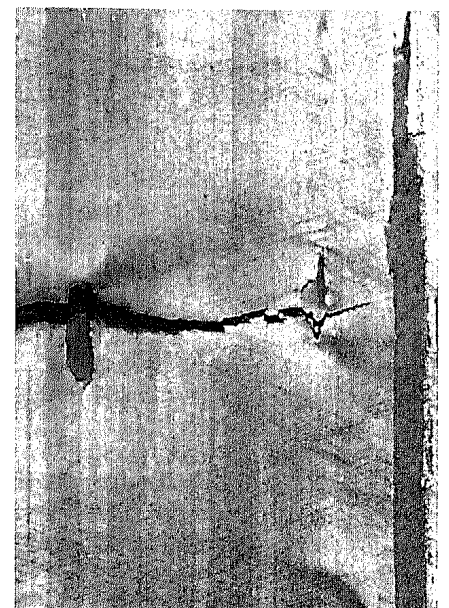Fig. 13b.   Formation of grain boundary cracks.

Fig. 13c.   Linkage of grain boundary cracks by transgranular cracks.

Fig. 13a to c.   Summary of transgranular fracture. (In all pictures the stress direction is vertical.)

The strain rate due to void growth can be written as[13]

$$\dot{\varepsilon}_c = \frac{4 \, \delta_B \, D_B \, \Omega \, \delta_c}{k \, T \, L \, \ln(1/f) \, z^2} \tag{A1}$$

where σ_c is the stress at the damaged grain boundary driving void growth. $\delta_B D_B$ is the grain boundary width times its diffusivity, Ω the atomic volume, k Boltzmann's constant and T the absolute temperature.

The strain rate in undamaged grains adjacent to damaged grain boundaries is due to power-law creep:

$$\dot{\varepsilon}_u = \dot{\varepsilon}_0 \left[\frac{\sigma_u}{\sigma_0} \right]^n \tag{A2}$$

σ_u is the stress carried by the undamaged cross-section. $\dot{\varepsilon}_0$, σ_0 and n are creep constants. Compatibility requires both strain rates to match:

$$\dot{\varepsilon}_c = \dot{\varepsilon}_u \tag{A3}$$

Force equilibrium obtains when

$$(2s - l) \, \sigma_u + l \, \sigma_c = 2s \, \sigma_\infty \tag{A4}$$

where σ_∞ is the applied tensile stress and $2s$ the spacing of damaged grain boundaries in transverse direction (see Fig. 11).

From a geometrical consideration we get:

$$2s = R \, l \tag{A5}$$

Equations (A1) to (A5) lead to an implicit equation for σ_c/σ_0:

$$\dot{\varepsilon}_0 \cdot \left[\frac{1}{(1-1/R)} \frac{\sigma_\infty}{\sigma_0} - \frac{1}{(R-1)} \frac{\sigma_u}{\sigma_0} \right]^n = \frac{4 \, \delta_B \, D_B \, \Omega \, \sigma_0}{k \, T \, L \, \ln(1/f) \, z^2} \frac{\sigma_c}{\sigma_0} \tag{A6}$$

with the following approximate solution:

$$\frac{\sigma_c}{\sigma_0} \approx \frac{\dfrac{1}{(1-1/R)} \left[\dfrac{\sigma_\infty}{\sigma_0} \right]^n}{\left[\dfrac{1}{(1-1/R)^n} - 1 \right] \left[\dfrac{\sigma_\infty}{\sigma_0} \right]^{n-1} + \dfrac{4 \, \delta_B \, D_B \, \Omega \, \sigma_0}{k \, T \, L \, \ln(1/f) \, \dot{\varepsilon}_0 \, z^2}} \tag{A7}$$

Using the equation for the damage rate df/dt (Ref. [13]):

$$\frac{df}{dt} = \frac{2 \, \delta_B \, D_B \, \Omega \, \sigma_0}{k \, T \sqrt{f} \, \ln(1/f) \, z^3} \cdot \frac{\sigma_c}{\sigma_0} \tag{A8}$$

we get the final equation for the rupture time:

$$t_f = \frac{k \, T \, z^3}{2 \, \delta_B \, D_B \, \Omega \, \sigma_0} \int_{f_i}^{f_c} \sqrt{f} \, \ln(1/f) \, \frac{\sigma_0}{\sigma_c} \, df \tag{A9}$$

where for σ_0/σ_c we use Eq. (A7). f_i is the initial damage (the value for $r_i > 2\gamma/\sigma$ where γ is the surface energy per unit area of the material) and f_c the damage at failure.

Integration of Eq. (A9) results in:

$$t_f = \frac{0.085 \, k \, T \, z^3}{\delta_B \, D_B \, \Omega \, \sigma_\infty} \, [1 - (1-1/R)^n] + \frac{\varepsilon_B}{\dot{\varepsilon}_u} (1-1/R)^n \tag{A10}$$

where the following boundary conditions have been applied:

$f_i \ll 0{,}01$ ($f_i \approx 0{,}0001$ for these tests)

$f_c < 1$ ($f_c = 0{,}25$; the choice of f_c is not very critical).

$\dot{\varepsilon}_u$ is the steady state strain rate and ε_B the strain to fracture due to the void growth. Integration of Eq. (A1) with dt =

$df/(df/dt)$ (for df/dt see Eq. (A8)) between the bounds f_i and f_c results in:

$$\varepsilon_B = \frac{z}{6L} \tag{A11}$$

Literature

1) G. H. GESSINGER, Powder Metallurgy of Superalloys, Butterworth, London (1984).
2) R. F. SINGER and E. ARZT, in High Temperature Alloys for Gas Turbines and Other Applications 1986, W. Betz, R. Brunetaud, D. Coutsouradis, H. Fischmeister, T. B. Gibbons, I. Kvernes, Y. Lindblom, J. B. Marriott, and D. B. Meadowcroft (eds.), Reidel, Dordrecht (1986) 97–126.
3) E. ARZT and D. S. Wilkinson, Acta Metall. 34 (1986) 1893.
4) E. ARZT, J. RÖSLER, and J. H. SCHRÖDER, in Creep and Fracture of Engineering Materials and Structures, B. Wilshire, R. W. Evans (eds.), The Institute of Metals, London (1987) 217.
5) E. ARZT and J. RÖSLER, Acta Metall. 36 (1988) 1043 and 1053.
6) R. L. CAIRNS, L. R. CURWICK, and J. S. BENJAMIN, Metall. Trans. 6A (1975) 179.
7) G. P. JONGENBURGER and R. F. SINGER, in Advanced Materials and Processing Techniques for Structural Applications, Proc. First ASM Europe Technical Conference, T. Khan and A. Lasalmonie (eds.), ONERA, Chatillon (1988) 339–348.
8) E. ARZT and R. F. SINGER, in Superalloys 1984, M. Gell et al. (eds.), AIME-TMS (1984) 367–376.
9) B. A. WILCOX and A. H. CLAUER, Acta Metall. 20 (1972) 743.
10) J. H. SCHRÖDER, "Elektronenmikroskopische Untersuchung des Hochtemperatur-Härtungsmechanismus in einer ODS-Superlegierung", Ph.D. Thesis, University of Stuttgart (1987), published in Fortschr.-Ber. VDI, Reihe 5 (1987) Nr. 131.
11) H. ZEIZINGER, "Werkstoffschädigung in einer ODS-Superlegierung durch Hochtemperaturermüdung und Kriechen", Ph.D. Thesis, University of Stuttgart (1986), published in Fortsch.-Ber. VDI, Reihe 5 (1987) Nr. 121.
12) H. ZEIZINGER and D. S. WILKINSON (1988), to be published.
13) A. C. F. COCKS and M. F. ASHBY, Progr. Mat. Sci. 27 (1982) 189.
14) B. F. Dyson, Metal Sci. 10 (1976) 349.
15) E. ARZT, Z. Metallkde. 75 (1984) 206.
16) H. RIEDEL, Fracture at High Temperatures, Springer-Verlag, Berlin (1987) Chap. 12.
17) T. E. HOWSON, D. A. MERVYN, and J. K. TIEN, Metall. Trans. 11A (1980) 1609.
18) E. ARZT, M. F. ASHBY, and R. A. VERRALL, Acta Metall. 31 (1983) 1977.
19) R. TIMMINS and E. ARZT, Scripta Metall. 22 (1988) 1353.
20) D. S. WILKINSON, Acta Metall. 35 (1987) 1251 and 2791.
21) H. RIEDEL, Z. Metallkde. 76 (1985) 669.
22) E. ARZT, D. ELZEY, and J. SCHRÖDER, in Advanced Materials and Processing Techniques for Structural Applications, Proc. First ASM Europe Technical Conference, T. Khan and A. Lasalmonie (eds.), ONERA, Chatillon (1988) 327–338.
23) D. ELZEY and E. ARZT, in Superalloys 1988, Proc. 6th Internat. Symp. on Superalloys, S. Reichman, D. N. Duhl, G. Maurer, S. Antolovich, and C. Lund (eds.), TMS (1988) 595–604.